UDK 621.396

VIRTUAL BEAMFORMING-BASED REGULARIZATION APPROACH FOR ENHANCED RADAR/SAR IMAGING

YURIY SHKVARKO, JOEL AMAO, AND ISRAEL YAÑEZ

To perform intelligent analysis of the radar remote sensing imagery acquired with conventional real aperture radar (RAR) or fractional synthetic aperture radar (F-SAR) sensor systems, the original low resolution speckle corrupted images must undergo feature enhancing processing. In this paper, such a processing task is treated as an uncertain nonlinear inverse problem of reconstruction of the scene power reflectivity map from a low resolution image formed employing conventional matched spatial filtering (MSF) of the trajectory data signals. The minimum variance distortionless response (MVDR) virtual adaptive beamforming method is first adapted to coherent RAR/F-SAR imaging modalities and is next restructured into the iterative reconstructive imaging technique that employs the descriptive experiment design regularization (DEDR) framework unified with the variational analysis inspired convergence guaranteed and sparsity promoting composite projectors onto the convex solution sets (POCS). The overall multilevel POCS regularized DEDR-restructured MVDR technique (addressed as the DEDR-MVDR method) performs feature enhanced reconstructive imaging via spatially selective despeckling balanced over the POCS regularized DEDR-optimal resolution enhancement with sparsity preservation. The DEDR-MVDR method implemented in an implicit iterative form does not involve cumbersome matrix inversions at all processing stages. The reported simulations corroborate the efficiency of the developed DEDR-MVDR technique especially in decreasing of the computational complexity without sacrificing the potentially attainable spatial resolution.

Keywords: beamforming, descriptive experiment design regularization, synthetic aperture radar, radar imaging, resolution.

INTRODUCTION

Modern imaging radar and synthetic aperture radar (SAR) systems can provide microwave images of terrestrial surfaces in different wavebands independent of weather conditions and sunlight illumination. The majority of conventional airborne monitoring or navigation missions use low cost real aperture radar (RAR) or fractional SAR (F-SAR) sensing systems. However, the fractional synthesis mode inevitably sacrifices spatial resolution and usually suffers from operational scenario uncertainties attributed to random signal perturbations in a turbulent atmosphere, imperfect system calibration, multiplicative speckle noise, and possible uncontrolled carrier trajectory deviations [1–4]. All low cost airborne RAR/F-SAR systems employ the so-called matched spatial filtering (MSF) based processing of the trajectory data signals in both the slant range and cross range (azimuth) directions performed over the "fast" and "slow" trajectory time scales, correspondingly, for image formation. The MSF method is sometimes referred to as a quick-look or compressed sensing mode [1, 7, 9], but despite its wide application it is able to produce only low resolution (i.e., blurred) imagery corrupted by both additive noise and multiplicative speckle. The mapping capabilities of such RAR/F-SAR sensors are insufficient to reach the goals of multi-purpose analysis of the provided imagery, which make the interpretation of the remotely sensed data very difficult and in some operational scenarios even impossible [3–7]. If the on-board coherent full aperture synthesis mode with further adaptive platform motion and atmospheric errors corrections are unavailable (as it is a case in all low cost remote sensing (RS) and autonomous navigation missions with RAR/F-SAR sensors), the challenging problem consists in an attempt to perform feature enhanced recovery of the low resolution (LR) radar imagery via it computational processing [3, 9–15]. The crucial problem relates to performing some space-time adaptive processing (STAP) of such degraded radar/F-SAR images to make them suitable for further intelligent data analysis and interpretation in particular RS applications. In the signal processing settings, such STAP tasks are traditionally addressed as feature enhanced radar image recovery that is basically aimed at considerable image resolution enhancement balanced over noise and speckle suppression. These tasks can be formalized in a framework of nonparametric inverse problems of reconstruction of the scattered field spatial spectrum pattern (SSP) i.e., estimation of the average scene power reflectivity referred to as a scene image [6, 11–17]. Representing a spatial map of the RS scene power reflectivity (i.e., the second-order statistics of the random backscattered field), the SSP may possess a local spatial sparsity property peculiar for some piecewise smooth scenes [7, 9, 12, 13]. The deficiency in the spatial resolution and presence of noise and speckle make the SSP recovery problem ill-posed [7, 11, 12, 13, 18, 19]. Modern approaches for solving such a class of uncertain nonlinear inverse problems are based on a combination (fusion) of some regularized image restoration/recovery techniques with adaptive de-speckling methods (e.g., see [5, 7, 11, 17–20] and the references therein). In harsh sensing environments, solution of the SSP recovery inverse problem is complicated due to the random perturbations in the signal formation operator (SFO) that cause multiplicative degradations (speckle) with the statistics (in general, non-Gaussian) usually unknown to the observer [5, 6, 11–14]. The restoration or recovery tasks are aimed at spatial resolution enhancement that needs performing of some approximated adaptive SFO inversion; the latter should also be balanced over suppression of the image-dependent speckle noise. The conventional multilook de-speckling approach [2–7] does not satisfy these requirements because it considerably sacrifices the spatial

resolution. There is a vast amount of literature on approaches that provide superior performances over the MSF method for SSP estimation when certain assumptions are met (e.g., see [3, 10–20] and the references therein).

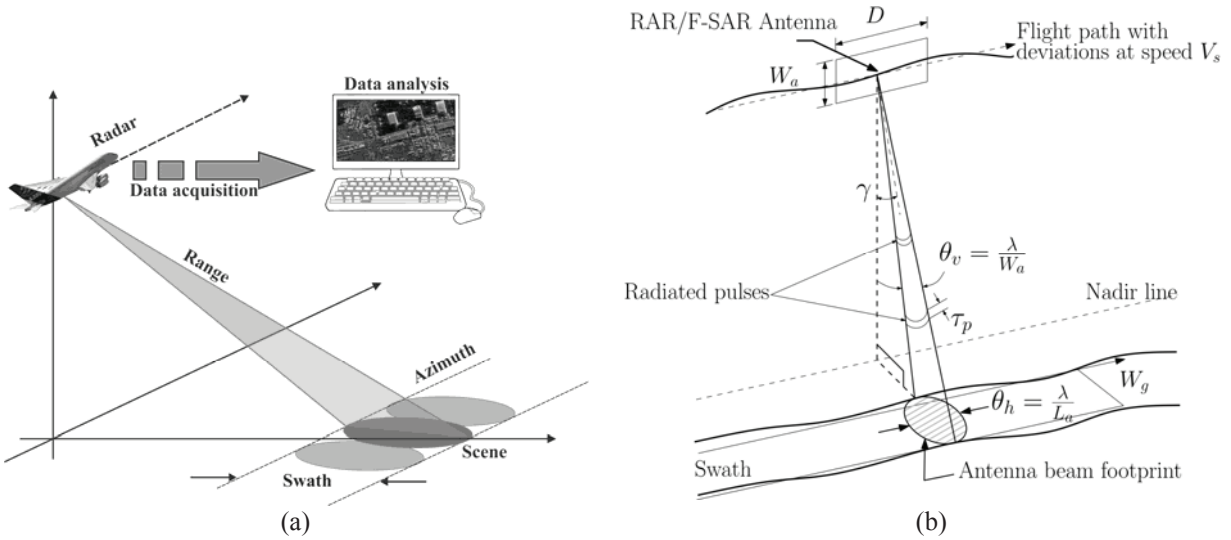

(a) (b)

Fig. 1: (a) Essential elements of a typical remote sensing imaging radar; (b) Geometry of a RAR/F-SAR imaging scenario with carrier trajectory deviations.

The most crucial restriction, however, relates to the featured above inverse problem nonlinearity and model uncertainty. Moreover, non-Gaussian statistics of speckle and SFO perturbations (usually unknown to the observer) make infeasible application of the Bayesian inference strategies [11–17] for SSP recovery. Some competing developments [7, 11, 14, 18, 20] argue to employ advanced digital beamforming techniques to improve the recovered image performances. However, the still unresolved problem relates to adaptation of the beamforming-based techniques to solving the inverse problems of feature-enhanced recovery of the scene SSP maps already provided with the LR RAR/F-SAR sensors.

In this study, we consider the nonlinear inverse problem of feature-enhanced SSP reconstruction from a coherent (complex) LR RAR/F-SAR images formed employing the conventional MSF processing method [2, 4, 8, 12]. The recovery problem is stated and treated in the descriptive experiment design regularization (DEDR) framework [12, 13] unified with the robust minimum variance distortionless response (MVDR) virtual beamforming approach [1, 18]. The new challenging propositions are threefold: (i) to solve the nonlinear inverse problem at hand with considerable resolution enhancement over noise suppression gains; (ii) to construct the solution in a form of an MVDR inspired virtual beamforming-based procedure that does not involve cumbersome data matrix inversions at all processing levels, and at the same time guarantees preservation of a sparsity of the recovered scene SSP (if exists); and (iii) to build an efficient iterative scheme for speeded-up implementation of the MVDR-based sparsity promoting SSP recovery procedure. To achieve these goals, we incorporate into the DEDR strategy for SSP reconstruction the additional convergence guaranteed composite projectors onto the convex solution sets (POCS) [11–13]. Next, we put the DEDR-POCS solution into the modified MVDR virtual beamforming framework that excludes matrix inversions at all processing levels. Last, we construct the implicit contractive mapping iterative scheme for efficient computational implementation of the developed POCS-regularized DEDR-restructured robust MVDR-based method for SSP recovery. In the reported simulations, we corroborate the effectiveness of our new DEDR-MVDR method in the resolution enhancement over noise suppression gains as well as in the convergence rates via its comparison with the competing feature-enhanced radar imaging techniques in the literature [1–7, 11–15].

The rest of the paper is organized as follows. The problem model that we treat in this paper is structurally similar to the previous studies [1, 9, 12, 13], thus the system-level and general phenomenological background and some numerical model details are repeated for convenience to the reader in Section I. In Section II, we develop our new DEDR–restructured virtual MVDR beamforming based technique (that we address here as the unified DEDR-MVDR method). Here, we also provide modifications of the DEDR-MVDR-based solution procedure to avoid cumbersome matrix inversions at all processing levels. Two processing schemes for computational implementation of the developed image recovery method are built in Section III. The algorithmic developments are followed by the effectiveness corroborative numerical simulations featured in Section IV. Concluding remarks in Section V summarize the addressed study.

I. Problem Phenomenology

A. Basics of a Radar Imaging System

Conventional low resolution real aperture radar (RAR) microwave imaging radar systems operate via forming fan shaped antenna beams, with wide radiated/received patterns in elevation, to illuminate a respectable swath width in range, and narrow azimuth antenna patterns, to accumulate the image line by line [1–5, 8, 11].

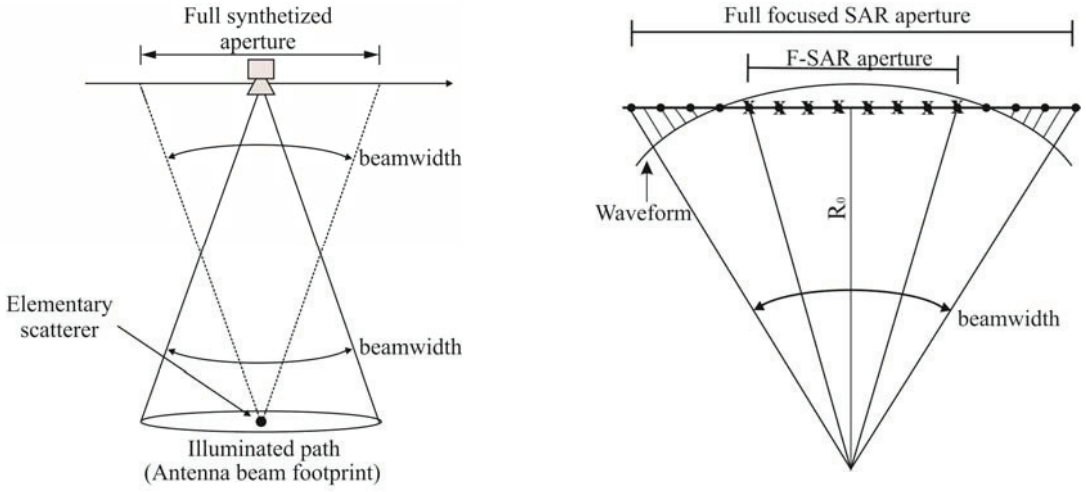

Fig. 2 (a) Full-focused synthetic aperture radar geometry; (b) Problem geometry for an unfocused and fractionally focused synthetic antenna modalities; R_0 represents the range from an elementary scattered target to the center of the synthesized array.

This is illustrated in Figure 1 (a). Imaging radars are differentiated between each other on how they achieve resolution in the range and azimuth directions. Resolution is a measure of image sharpness; the minimum distance two objects (elementary scatterers) have to have in order that their echoes are separable. In the real-world airborne RS scenarios, the carrier flight trajectory is not always nominal; there can be uncontrolled (modeled as unknown deterministic or random) deviations from the nominal flight trajectory (the carrier deviations) during the flight time, changes in the flight altitude, imperfect radar calibrations, etc. Figure 1(b) illustrates these effects peculiar for a RAR/F-SAR system. Here, the radar system is aboard a platform moving at a speed V_s in a non-nominal trajectory, γ defines the angle between the radar beam and the normal line to the earth surface in a particular point of interest, τ_p defines the duration of the radar impulse width, θ_v is the width of the vertical radar beam, θ_h indicates the antenna beam footprint, W_a represents the effective antenna height, D is the effective antenna length, and W_g represents the swath width.

In the systems that employ simple pulse modulated signals, the slant range resolution is determined by the pulse duration [2–4, 8]. The technical way to increase range resolution capability is to employ chirp modulated pulses that admit efficient pulse compression via performing MSF of the trajectory signals in the range direction [2, 4, 8]. Such sensing modality provides sufficiently high range resolution capabilities evaluated for the chirp modulated pulse signals as $\delta_{\text{range}} = (1.4c)/(2\pi B)$ [8] where c represents the speed of propagation of electromagnetic waves and B is the chirp signal bandwidth. Thus, the range resolution problem is technically resolved employing chirp pulse compression techniques, e.g., [2–4, 8]. The crucial problem, on the other hand, relates to the low azimuth (cross range) resolution attainable with conventional RAR sensors [1–5, 8, 11]. The technical way to increase the azimuth resolution is to synthesize the antenna aperture, well known as SAR sensing, e.g., [2–4, 7, 8], etc. Thus, the azimuth resolution depends on the particular mode of the trajectory data signals recording employed in a particular sensing scenario. Here beneath, to complete the background, we feature three general radar sensing modalities that affect the overall azimuth resolution capabilities.

B. System-Level Limitations on Azimuth Resolution

Three typical trajectory data acquisition modes affect the resulting azimuth resolution capability [2, 3, 8].

1) The conventional RAR modality with MSF trajectory signal processing provides azimuth resolution strictly dependent upon the width of the radiated beam [2, 3, 8].

2) The so-called unfocused synthetic antenna modality (unfocused SAR) is able to perform some aperture synthesis, in which the synthetic antenna length is made as long as the unfocused technique permits [4, 8].

3) In the focused synthetic antenna mode, the synthesized array length can be made equal to the back projected linear width of the radiated beam at each range gate (potential, so-called full-focused modality) or its fraction (fractionally-focused modality).

The linear azimuth resolution for the conventional RAR case is given by [2, 8]

$$\delta_{a(\text{RAR})} = \frac{\lambda R}{D}. \quad (1)$$

For the unfocused F-SAR modality, the linear azimuth resolution is defined as [8]

$$\delta_{a(\text{unf SAR})} = \frac{1}{2}\sqrt{\lambda R}, \quad (2)$$

whereas for the full-focused SAR, the resolution is increased to its potentially attainable value [2]

$$\delta_{a(\text{foc SAR})} = \beta_{\text{eff-max}} R = \frac{D}{2}. \quad (3)$$

Here λ represents the wavelength of the radar signal transmitted, D is the horizontal aperture length of a physical antenna, R is the range to the scattering element

on the scene (related to a particular considered range gate), $\beta_{\text{eff}} = \lambda/2L_{\text{eff}}$ represents the effective half-power beamwidth of the synthetic aperture, and L_{eff} is the length of the synthetic aperture. For the full focused mode, L_{eff} equals to the back projected antenna footprint width, i.e., $L_{\text{eff}} = L_{\text{eff-max}} = R\lambda/D$ that results in the potentially attainable azimuth resolution (3).

Clear that in the conventional RAR modality, for achieving moderate azimuth resolution a very narrow beam should be radiated. The half-power beamwidth $\beta_{\text{eff(RAR)}} = \lambda/D$ produces the linear azimuth resolution (1), i.e., the product of beamwidth λ/D with the range R. In the unfocused SAR modality, the conventional data processing technique performs MSF of the trajectory signal acquired within the unfocused synthetic aperture [2–5, 8]. In this case, the coherent signals received at the synthetic array points are integrated, with no attempt made to shift the phases of the signals before integration [8]. This lack of phase adjustment imposes a limitation on the maximum open/unfocused synthetic antenna length that can be generated. This maximum unfocused synthetic antenna length occurs at a given range when the round-trip distance from a radar target to the center of the synthetic array differs no greater than by $\lambda/4$ from the round-trip distance between the radar target and the extremities of the unfocused synthetic aperture array that result in the linear azimuth resolution given by (2) [8] as examplified in Fig. 2.

Last, in the fractional focused SAR (F-SAR) modality (see Fig. 2(b)), only a fraction (say, $\alpha < 1$) of the potential full-focused aperture $L_{\text{eff}} = \alpha L_{\text{effmax}} = \alpha R\lambda/D$ is employed to coherently register the trajectory signals for further MSF processing, hence the linear azimuth resolution attainable employing the conventional MSF processing is a $1/\alpha$ coarser than the potential value (3), i.e.,

$$\delta_{a(\text{F-SAR})} = \frac{D}{2\alpha};\ \alpha < 1. \tag{4}$$

Next step is to cast and treat the problem of feature enhanced radar imaging via processing of the trajectory data signal coherently registered with a RAR, F-SAR, or unfocused SAR sensors (the latter can also be viewed as a particular F-SAR modality) in the framework of image recovery inverse problems.

C. General Radar Imaging Problem Formalism

Referring to the previous related studies [1, 9, 12, 13] consider a coherent remote sensing (RS) experiment with a narrowband RAR/F-SAR imaging system that enables us to model the extended scene backscattered field by imposing its time invariant complex scattering function $v(\mathbf{r})$ in the scene domain (scattering surface) Rэ$\mathbf{r}$. The measurement data wavefield $u(\mathbf{p})=s(\mathbf{p})+n(\mathbf{p})$ consists of the echo signals s and additive noise n and is assumed to be available for observations and recordings within the prescribed time-space observation domain Pэ$\mathbf{p}$, where $\mathbf{p} = (t, \boldsymbol{\rho})^{\mathrm{T}}$ defines the time-space points in the trajectory observation domain $P=T\times\mathrm{P}$. The model of the RAR/F-SAR trajectory data signal u is defined by specifying the linear stochastic equation of observation (EO) of an operator form [12], $u = \tilde{\boldsymbol{\mathcal{S}}}v + n$; $v \in \mathbb{V}$; $u,\ n \in \mathbb{U}$; $\tilde{\boldsymbol{\mathcal{S}}}: \mathbb{V} \to \mathbb{U}$, in the Hilbert spaces $\mathbb{V}$ and $\mathbb{U}$ with the $\mathbb{L}_2$ metrics structures induced by the scalar products [11]

$$[u_1, u_2]_{\mathbb{U}} = \int_P u_1(\mathbf{p})u_2^*(\mathbf{p})d\mathbf{p};\quad \mathbf{p} \in P \quad \text{and}$$

$$[v_1, v_2]_{\mathbb{V}} = \int_R v_1(\mathbf{r})v_2^*(\mathbf{r})d\mathbf{r};\quad \mathbf{r} \in R, \tag{5}$$

respectively. In the conventional integral-form representation format, the observation trajectory signal $u(\mathbf{p})$ is expressed as

$$u(\mathbf{p}) = \int_R \tilde{S}(\mathbf{p},\mathbf{r})v(\mathbf{r})d\mathbf{r} + n(\mathbf{p});$$
$$v(\mathbf{r}) \in \mathbb{V}(R);\ u(\mathbf{p}), n(\mathbf{p}) \in \mathbb{U}(P), \tag{6}$$

where $\tilde{S}(\mathbf{p},\mathbf{r})$ represents the functional kernel of the perturbed SFO $\tilde{\boldsymbol{\mathcal{S}}}: \mathbb{V} \to \mathbb{U}$. Its mean, $\boldsymbol{\mathcal{S}} = <\tilde{\boldsymbol{\mathcal{S}}}>$; $\boldsymbol{\mathcal{S}}: \mathbb{V} \to \mathbb{U}$, is completely specified by the regular kernel component given by the averaging $S(\mathbf{p},\mathbf{r}) = <\tilde{S}(\mathbf{p},\mathbf{r})>$ (over the randomness of $\tilde{\boldsymbol{\mathcal{S}}}: \mathbb{V} \to \mathbb{U}$) that is defined by the employed signal wavefield formation model [4, 11, 12]. Such regular SFO kernel $S(\mathbf{p},\mathbf{r})$ is fully determined by the time-space modulation of signals employed in a particular radar system [5, 11, 12]. The variation about the mean, $\boldsymbol{\Delta}_{\boldsymbol{\mathcal{S}}} = \tilde{\boldsymbol{\mathcal{S}}} - \boldsymbol{\mathcal{S}}$, models perturbations of the wavefield at different propagation paths. In different problem model treatments, such SFO perturbation component, $\boldsymbol{\Delta}_{\boldsymbol{\mathcal{S}}}$, can be considered as unknown deterministic or random. In the stochastic model treatment, $\boldsymbol{\Delta}_{\boldsymbol{\mathcal{S}}}$ is characterized by the general Rytov's statistical model [5].

Following the above operator observation model formalism, we next assume an incoherent nature of the extended object/scene scattered wavefield $v(\mathbf{r}) \in \mathbb{V}(R)$. This is naturally inherent to all real-world radar RS scenarios [2, 5, 11, 12] and leads to the δ-form of the scattered wavefield correlation function

$$R_v(\mathbf{r}_1,\mathbf{r}_2) = <v(\mathbf{r}_1)v^*(\mathbf{r}_2)> = b(\mathbf{r}_1)\delta(\mathbf{r}_1 - \mathbf{r}_2);$$
$$b(\mathbf{r}) = <|v(\mathbf{r})|^2>;\quad \mathbf{r},\ \mathbf{r}_1, \mathbf{r}_2 \in R \tag{7}$$

where $v(\mathbf{r})$ and $b(\mathbf{r}) = <|v(\mathbf{r})|^2>$ are referred to as the scene random complex reflectivity and its average power reflectivity/scattering function or spatial spectrum pattern (SSP), respectively. In the standard settings, $v(\mathbf{r})$ is modeled as a zero mean random Gaussian field [2, 5], while the statistics of $u(\mathbf{p})$ depend on the employed statistical models of additive noise $n(\mathbf{p})$ and the SFO perturbations.

The considered here RS imaging problem is formally stated as follows: to derive an estimate $\hat{b}(\mathbf{r})$ of the scene SSP $b(\mathbf{r})$ (referred to as the desired RS power image) by processing the available finite dimensional RAR/F-SAR measurements of the trajectory data signal $u(\mathbf{p})$. It is clear that any feasible estimator of $\hat{b}(\mathbf{r})$ must involve a solution of the operator equation of observation (6) optimal/suboptimal in the sense of some posed criterion. Such a solution assumes inversion (or some approximated in-

version/pseudo-inversion) of the SFO, with the desired SSP estimate related to the complex scattering function via the second order statistical model (7). Thus, such a problem falls into a class of stochastic nonlinear inverse problems. Moreover, due to the SFO perturbations (modeled as unknown deterministic or stochastic with statistics usually unknown to the observer), the problem at hand should be treated as an uncertain stochastic nonlinear inverse problem. Note that random SFO model makes the statistics of the observation signal $u(\mathbf{p})$ non-Gaussian (and unknown to the observer). This makes unfeasible application of the Bayesian inference strategies. Hence some non-Bayesian regularization-based problem solvers should be developed and applied.

D. Problem Model

Following standard trajectory signal discretization schemes [3, 4, 12] consider the vector-form approximation

$$\mathbf{u} = \tilde{\mathbf{S}}\mathbf{v} + \mathbf{n} = \mathbf{S}\mathbf{v} + \mathbf{\Delta}_{\mathbf{S}}\mathbf{v} + \mathbf{n}, \qquad (8)$$

of the integral equation of observation (6). Here, vector $\mathbf{v}$ represents the lexicographically ordered pixel-format representation of the random scene reflectivity function $v(\mathbf{r})$ observed through the $M\times K$ perturbed matrix-form SFO $\tilde{\mathbf{S}} = \mathbf{S} + \mathbf{\Delta}_{\mathbf{S}}$ and contaminated by additive Gaussian noise vector $\mathbf{n}$. The discrete-form SFO, $\tilde{\mathbf{S}} = \mathbf{S} + \mathbf{\Delta}_{\mathbf{S}}$, is the $M\times K$ ($M<K$ for compressed sensing scenarios) matrix-form approximation of the integral-form perturbed SFO $\tilde{\mathcal{S}}: \mathbb{V} \to \mathbb{U}$, in which the regular component $\mathbf{S}$ is specified by the employed modulation and synthesis mode [3, 4, 12]. In (8), $\mathbf{v}$, $\mathbf{n}$, $\mathbf{u}$ are treated as zero-mean random vectors composed of the entries $\{v_k\}_{k=1}^{K}$, $\{n_m\}_{m=1}^{M}$ and $\{u_m\}_{m=1}^{M}$ of the discrete-form approximations of the fields u, n and v with respect to the employed orthogonal decomposition function set $\{h_m(\mathbf{p})\}$ in the observation domain and the expansion (pixel) set $\{g_k(\mathbf{r})\}$ in the scene domain, respectively [3, 4, 8]. These vectors are characterized by the correlation matrices, $\mathbf{R}_{\mathbf{v}} = \mathbf{D}(\mathbf{b}) = \mathrm{diag}(\mathbf{b})$, the diagonal matrix with the vector-form SSP $\mathbf{b}$ at its principal diagonal, $\mathbf{R}_{\mathbf{n}} = N_0\mathbf{I}$ and $\mathbf{R}_{\mathbf{u}} = <\tilde{\mathbf{S}}\mathbf{R}_{\mathbf{v}}\tilde{\mathbf{S}}^{+}> + N_0\mathbf{I}$, correspondingly, where the averaging $<\cdot>$ is performed over the randomness of perturbations $\mathbf{\Delta}_{\mathbf{S}}$ of the regular SFO $\mathbf{S}$. In (8), superscript $^{+}$ stands for Hermitian conjugate (adjoint operator [11]), and N_0 is the white observation noise power $\mathbf{n}$. Vector $\mathbf{b}$ represents a lexicographically ordered by multi index $k = (k_x, k_y)$ vector-form representation of the SSP map $\mathbf{B} = \{b(k_x, k_x)\}$ over the $K_y\times K_x$ pixel-framed 2-D scene $\{k_x = 1,\ldots, K_x;\ k_y = 1,\ldots, K_y;\ k = 1,\ldots, K = K_xK_y\}$ [12, 17]. The matrix-form representation of the uncertain SFO in (4) is given by [13]

$$\tilde{\mathbf{S}} = \mathbf{S} + \mathbf{\Delta}_{\mathbf{S}}, \qquad (9)$$

in which the $M\times K$ nominal SFO matrix $\mathbf{S}$ is composed of the scalar products $\{[Sg_k, h_m]_{\mathbb{U}};\ k = 1, \ldots, K;\ m = 1, \ldots, M\}$ [11] while all problem model uncertainties are attributed to the distortion term $\mathbf{\Delta}_{\mathbf{S}}$. In the stochastic treatment, such $\mathbf{\Delta}_{\mathbf{S}}$ is modeled as a random zero-mean matrix with the bounded second-order moment, i.e.

$$<\mathbf{\Delta}_{\mathbf{S}}> = \mathbf{0};\ \ <\|\mathbf{\Delta}_{\mathbf{S}}\|^2> = \langle \mathrm{tr}\{\mathbf{\Delta}_{\mathbf{S}}\mathbf{\Delta}_{\mathbf{S}}^{+}\}\rangle \le \eta \qquad (10)$$

where $\|\mathbf{\Delta}_{\mathbf{S}}\|^2 = \mathrm{tr}\{\mathbf{\Delta}_{\mathbf{S}}\mathbf{\Delta}_{\mathbf{S}}^{+}\}$ defines the squared Frobenius matrix norm, $\mathrm{tr}\{\cdot\}$ is the trace operator, superscript $^{+}$ defines the Hermitian conjugate (conjugate transpose), and η is the bounding constant [12] that we consider as a user specified problem model parameter. In the limiting case, $\eta = 0$, the SFO perturbations are neglected, hence the problem is simplified to the certain nonlinear inverse problem with Gaussian statistics of all vectors in (8).

E. Discrete-Form Imaging Problem Formalism

A solver to the nonlinear inverse problem for recovery of the SSP vector $\mathbf{b}$ from the available data recordings $\mathbf{u}$, i.e.,

$$\hat{\mathbf{b}} = est_{strategy}\{\mathbf{b} \mid \mathbf{u}\} \qquad (11)$$

obviously depends on the employed estimation *strategy*.

For the commonly accepted Gaussian model [3] of the complex reflectivity $\mathbf{v}$ and random (Gaussian or non-Gaussian [3, 4, 11]) SFO perturbations term $\mathbf{\Delta}_{\mathbf{S}}$ in (9), the composite noise, $\mathbf{\Delta}_{\mathbf{S}}\mathbf{v} + \mathbf{n}$, in (8) is, in general, non-Gaussian distributed and signal dependent [1, 7, 11], and it is not even practical to model it as a mixture of Gaussians due to insufficient training data and the lack of knowledge about the number of Gaussian mixtures [11]. This makes infeasible application of the Bayesian estimation strategy.

The feasible competing approach that we propose to follow in this study is based on the worst case statistical performances optimization adapted minimum risk inspired DEDR framework [12] that does not require knowledge of the particular probabilistic characteristics of the data model (8). The general-form DEDR solver $\hat{\mathbf{b}} = est_{\mathrm{DEDR}}\{\mathbf{b} \mid \mathbf{u}\}$ seeks for an SSP estimate in the positive convex cone solution set in the Euclidian image/solution space $\mathbb{B}_{(K)}$ with the metric structure induced by the generalized $\ell_2 - \ell_2$ scalar products [13]

$$\|\mathbf{b}\|^2_{\mathbb{B}_{(K)}} = [\mathbf{b}, \mathbf{b}] + [\nabla\mathbf{b}, \nabla\mathbf{b}] = [\mathbf{b}, (\mathbf{I} + \nabla^2)\mathbf{b}] \qquad (12)$$

which involves equibalanced ℓ_2 structured image norm and image gradient norm. In our metrics construction (12), operator ∇ is defined via the square root of the discrete-form Laplace operator ∇^2 [11], hence $\nabla\mathbf{b}$ returns the K-D equivalent of the image gradient [11]. After the desired SSP vector estimate (11) in the properly structured solution space $\mathbb{B}_{(K)} \ni \mathbf{b}, \hat{\mathbf{b}}$ is found, the final SSP distribution is reconstructed via the composition

$$\hat{b}_{(K)}(\mathbf{r}) = \sum_{k=1}^{K} \hat{b}_k g_k(\mathbf{r}) \qquad (13)$$

over the pixel-framed observation scene specified by the employed set of pixels (usually rectangular) $\{g_k(\mathbf{r}); \mathbf{r} \in R\}_{k=1}^{K}$.

The feature enhanced RS imaging problem at hand is to develop the framework (in this study, the unified POCS-regularized DEDR-restructured MVDR method) and the related technique(s) for high-resolution estimation (feature-enhanced reconstruction) of the SSP as a solution to the following nonlinear inverse problem

$$\hat{\mathbf{b}} = est_{\text{DEDR-MVDR}}\{\mathbf{b} \mid \mathbf{u} = \tilde{\mathbf{S}}\mathbf{v} + \mathbf{n};\ \mathbf{R}_{\mathbf{v}} = \text{diag}(\mathbf{b})\} \quad (14)$$

via processing the available recordings (8) of the complex (coherent) trajectory data $\mathbf{u}$ degraded by the composite noise (multiplicative $\mathbf{\Delta}_{\mathbf{S}}$ and additive $\mathbf{n}$) with the SFO perturbation statistics $<\tilde{\mathbf{S}}\mathbf{R}_{\mathbf{v}}\tilde{\mathbf{S}}^{+}>$ unknown to the observer.

The DEDR framework developed in the previous studies [12, 13] provides the solution to the generic SSP recovery problem (11) that is feasible only for non-sparse SSP vectors. Moreover, such method involves cumbersome regularized inversions of the matrix-form point spread function (PSF) operators, in which the regularizer $(\text{diag}(\mathbf{b}))^{-1}$ is feasible for non-sparse SSP vectors $\mathbf{b}$ only. To treat competing operational scenarios with sparse SSP vectors $\mathbf{b}$ the new modified version of the DEDR strategy that does not involve inversions $(\text{diag}(\mathbf{b}))^{-1}$ should be conceived. In this study, we propose to follow the DEDR-restructured MVDR strategy, and develop the solvers that completely exclude matrix inversions at all solution stages.

II. Modified DEDR-MVDR Method

A. Adaptation of Robust MVDR Beamforming for Radar Imaging

The classical robust adaptive MVDR method adapted for the high resolution nonparametric radar imaging defines the estimates of all SSP vector entries via the square detected $(\{\cdot\}_{\text{SQ-DET}})$

$$\{\ \hat{b}_k = \{[\mathbf{u}, \mathbf{w}_k(\hat{\mathbf{b}})]\}_{\text{SQ-DET}}\ \forall\ k = 1,..., K\ \} \quad (15)$$

adaptive beamformer outputs computed as inner products $\{[\mathbf{u}, \mathbf{w}_k(\hat{\mathbf{b}})];\ k = 1,..., K\}$ of the data vector $\mathbf{u}$ with the so-called optimal beamformer weight vectors $\{\ \mathbf{w}_k(\hat{\mathbf{b}});\ k = 1,..., K\ \}$ [9, 18]. Those are solution-dependent; hence optimal adaptive processing is performed. Particular structures of the weight vectors $\{\mathbf{w}_k(\hat{\mathbf{b}})\}$ depend on the employed statement of the relevant optimal beamforming problem. In the most general robust MVDR setting [18], such $\{\mathbf{w}_k(\hat{\mathbf{b}})\}$ are defined via solving the following convex constrained optimization problem

$$\{(1/2) <|[\mathbf{u}, \mathbf{w}_k]|^2> \rightarrow \min_{\mathbf{w}_k} \quad \text{subject to } \{[\mathbf{s}_k, \mathbf{w}_k] = 1 \quad \text{for all look directions } k = 1,\ldots,K\} \quad (16)$$

where $\{\mathbf{s}_k;\ k = 1,\ldots,K\}$ are the corresponding column vectors of the regular SFO matrix $\mathbf{S}$. In the STAP signal processing terminology, those $\{\mathbf{s}_k;\ k = 1,\ldots,K\}$ are referred to as so-called steering vectors [18]. Later on, we will explain the MSF processing related sense of such steering vectors. Solution to the problem (16) yields the closed-form expressions to the optimal weight vectors [9, 18]

$$\{\mathbf{w}_k(\hat{\mathbf{b}}) = \alpha_k \mathbf{R}_{\mathbf{u}}^{-1}\mathbf{s}_k;\ k = 1,\ldots \text{K}\} \text{ with optimal scaling factors } \{\alpha_k = (\mathbf{s}_k^{+}\mathbf{R}_{\mathbf{u}}^{-1}\mathbf{s}_k)^{-1};\ k = 1,\ldots \text{K}\}. \quad (17)$$

Note that all weight vectors defined by (17) are solution-depended due to the dependence of the data theoretical covariance matrix $\mathbf{R}_{\mathbf{u}} = \mathbf{R}_{\mathbf{u}}(\mathbf{b}) = \mathbf{S}\text{diag}(\mathbf{b})\mathbf{S}^{+} + \mathbf{R}_{\mathbf{n}}$ on the SSP vector $\mathbf{b}$. Putting vectors (17) into (15) yields the nonlinear solution-dependent SSP estimator [9, 18]

$$\{\hat{b}_k = \frac{1}{\mathbf{s}_k^{+}\mathbf{R}_{\mathbf{u}}^{-1}(\mathbf{b})\mathbf{s}_k}\ ;\ \kappa = 1, ..., K\} \quad (18)$$

optimal (in the MVDR sense) for the theoretical model-dependent ($\mathbf{b}$-dependent) covariance matrix inverse $\mathbf{R}_{\mathbf{u}}^{-1}(\mathbf{b})$ where now $\mathbf{s}_k^{+}$ defines the kth steering vector composed of the corresponding kth row ($k = 1,\ldots, K$) of the adjoint regular SFO matrix $\mathbf{S}^{+}$ [12]. In the practical RS imaging scenarios, the unknown exact (model) covariance matrix $\mathbf{R}_{\mathbf{u}}(\mathbf{b})$ is substituted by its J-sample maximum likelihood (ML) estimate [1] $\mathbf{Y} = \hat{\mathbf{R}}_{\mathbf{u}} = (1/J)\sum_{j=1}^{J}\mathbf{u}_{(j)}\mathbf{u}^{+}_{(j)}$ that results in the corresponding MVDR algorithm for SSP estimation [18]

$$\{\hat{b}_k = \frac{1}{\mathbf{s}_k^{+}\mathbf{Y}^{-1}\mathbf{s}_k};\ k = 1,\ldots, K\} \quad (19)$$

feasible for the full rank estimated data covariance matrix $\mathbf{Y}$ only.

B. DEDR-Restructured Robust MVDR Technique for Enhanced SSP Reconstruction

From simple algebra, it is easy to corroborate that the theoretical model-based MVDR estimator (18) is algorithmically equivalent to the solution (with respect to the SSP vector $\mathbf{b}$) of the nonlinear equation

$$\hat{\mathbf{b}} \rightarrow \text{solution to the Eq.} \rightarrow \{\mathbf{D}(\mathbf{b})\}_{\text{diag}} = \{\mathbf{W}(\mathbf{b})\mathbf{R}_{\mathbf{u}}(\mathbf{b})\mathbf{W}(\mathbf{b})\}_{\text{diag}} \quad (20)$$

with the solution operator (SO)

$$\mathbf{W}(\mathbf{b}) = (\mathbf{D}(\mathbf{b})\mathbf{S}^{+}\mathbf{S} + N_0\mathbf{I})^{-1}\mathbf{D}(\mathbf{b})\mathbf{S}^{+}. \quad (21)$$

Substituting in (20) the theoretical covariance matrix $\mathbf{R}_{\mathbf{u}}$ by its sample estimate $\mathbf{Y} = \hat{\mathbf{R}}_{\mathbf{u}}$ yields the following DEDR-restructured MVDR strategy

$$\hat{\mathbf{b}} \rightarrow \text{solution to the Eq.} \rightarrow \hat{\mathbf{b}} = \{\mathbf{D}(\hat{\mathbf{b}})\}_{\text{diag}} = \{\mathbf{W}(\hat{\mathbf{b}})\mathbf{Y}\mathbf{W}(\hat{\mathbf{b}})\}_{\text{diag}} = \{\mathbf{A}(\hat{\mathbf{b}})\mathbf{Q}\mathbf{A}(\hat{\mathbf{b}})\}_{\text{diag}} \quad (22)$$

with the solution independent sufficient statistics (SS) matrix $\mathbf{Q} = \mathbf{S}^{+}\mathbf{Y}\mathbf{S}$ and the solution-dependent reconstruction matrix operator

$$\mathbf{A} = \mathbf{A}(\hat{\mathbf{b}}) = (\mathbf{D}(\hat{\mathbf{b}})\mathbf{\Psi} + N_0\mathbf{I})^{-1}\mathbf{D}(\hat{\mathbf{b}}). \quad (23)$$

In (21), (22), operator $\{\cdot\}_{\text{diag}}$ returns the vector of the principal diagonal of the embraced matrix, and in (23), $\mathbf{\Psi} = \mathbf{S}^{+}\mathbf{S}$ represents the matrix-form ambiguity function operator of the MSF linear low-resolution complex image formation system [1, 12, 13]. Note that in the DEDR-restructured MVDR estimator (22), matrix $\mathbf{A} = \mathbf{A}(\hat{\mathbf{b}})$ defined by (23) does not involve inversion of $\mathbf{D}(\hat{\mathbf{b}})$, hence, the solver to (22) results in the desired sparsity preserving DEDR-MVDR-optimal technique that admits zero entries (sparsity) in the SSP vector.

To adapt the solver (22) to the uncertain model of the perturbed SFO operator (9), we now follow the generic DEDR framework [12]. It suggests the robust approach for adjusting the SO (21) to the worst case statistical performances (WCSP) optimization model of the DEDR problem that yields the so-called robustified SO of the 2nd kind [12]

$$\mathbf{W}(\hat{\mathbf{b}}) = \mathbf{A}(\hat{\mathbf{b}})\mathbf{S}^{+} = (\mathbf{D}(\hat{\mathbf{b}})\mathbf{\Psi} + N_{\Sigma}\mathbf{I})^{-1}\mathbf{D}(\hat{\mathbf{b}})\mathbf{S}^{+} \qquad (24)$$

with the regularizing factor defined as a composite noise power $N_{\Sigma} = N_0 + \beta$, the additive observation noise power N_0 augmented by the loading factor $\beta \geq 0$ adjusted to the regular SFO Loewner ordering factor and its statistical uncertainty bound η specified in (10) (see [12] for details). Hence, the robust modification of the DEDR-MVDR estimator (22) is now constructed simply by replacing in (21), (23) N_0 by the composite (loaded) regularizing factor $N_{\Sigma} = N_0 + \beta$. In practical estimation scenarios, the diagonal loading factor β can be put spatially varying over the scene and evaluated empirically from the speckle-corrupted low-resolution MSF image following one of the local statistics methods exemplified in [12].

Now, we are ready to adapt the robust sparsity preserving DEDR-MVDR solver defined by (20), (24) to the considered here single look F-SAR mode ($J = 1$) via substituting $\mathbf{Y}$ by $\mathbf{u}\mathbf{u}^{+}$ and defining the complex MSF imaging system output

$$\mathbf{q} = \mathbf{S}^{+}\mathbf{u}, \qquad (25)$$

in which case, the robust sparsity preserving DEDR-MVDR solver (20), (24) yields the solution in the form of the elementwise square detected (SQ-DET) output of the reconstructive operator $\mathbf{A}(\hat{\mathbf{b}})$ applied to the complex MSF image $\mathbf{q}$, i.e.,

$$\hat{\mathbf{b}} \rightarrow \text{solution to the Eq.} \rightarrow \hat{\mathbf{b}} = \{\mathbf{A}(\hat{\mathbf{b}})\mathbf{q}\}_{\text{SQ-DET}} = \{\mathbf{A}(\hat{\mathbf{b}})\mathbf{q}\mathbf{q}^{+}\mathbf{A}(\hat{\mathbf{b}})\}_{\text{diag}}. \qquad (26)$$

with the restructured (diagonal loaded)

$$\mathbf{A} = \mathbf{A}(\hat{\mathbf{b}}) = (\mathbf{D}(\hat{\mathbf{b}})\mathbf{\Psi} + N_{\Sigma}\mathbf{I})^{-1}\mathbf{D}(\hat{\mathbf{b}}) \qquad (27)$$

From simple algebra, it is easy to corroborate that for the adopted single-look RAR/F-SAR modalities with the real-valued signal independent sufficient measurement statistics

$$\mathbf{Q} = \text{diag}(\mathbf{g}); \ \mathbf{g} = \{\mathbf{q}\}_{\text{SQ-DET}} \qquad (28)$$

available for further processing (i.e., the square detected low resolution MSF output (25)), the estimator (26) is algorithmically equivalent to the following DEDR-modified robust MVDR solver

$$\hat{\mathbf{b}} \rightarrow \text{solution to the Eq.} \rightarrow \ \mathbf{\Phi}(\hat{\mathbf{b}})\hat{\mathbf{b}} = \mathbf{D}^{2}(\hat{\mathbf{b}})\mathbf{g} = \mathbf{f} \qquad (29)$$

with the solution-depended weighted MSF data vector

$$\mathbf{f} = \mathbf{f}(\hat{\mathbf{b}}) = \mathbf{D}^{2}(\hat{\mathbf{b}})\mathbf{g}, \qquad (30)$$

and the solution-dependent MSF imaging system point spread function (PSF) matrix-form operator

$$\mathbf{\Phi} = \mathbf{\Phi}(\hat{\mathbf{b}}) = (\mathbf{D}(\hat{\mathbf{b}})\mathbf{\Psi} + N_{\Sigma}\mathbf{I}) \bullet (\mathbf{D}(\hat{\mathbf{b}})\mathbf{\Psi} + N_{\Sigma}\mathbf{I})^{*} \qquad (31)$$

where symbol $\bullet$ defines the Schur-Hadamard (elementwise) matrix product.

III. Implementation Schemes

A. POCS Regularized Iterative-Form Implementation

The next stage of our design consists in construction of the sparsity promoting POCS operator and its incorporation into (29) that yields the resulting POCS-regularized DEDR-restructured robust MVDR-optimal solver

$$\hat{\mathbf{b}} \rightarrow \text{solution to the Eq.} \rightarrow \ \mathcal{P}\{\mathbf{\Phi}(\hat{\mathbf{b}})\hat{\mathbf{b}} = \mathbf{D}^{2}(\hat{\mathbf{b}})\mathbf{g} = \mathbf{f}\} \qquad (32)$$

with the solution-dependent robust reconstructive operator $\mathbf{A} = \mathbf{A}(\hat{\mathbf{b}})$ defined by (27) and the composite POCS operator $\mathcal{P} = \mathcal{P}_3\mathcal{P}_2\mathcal{P}_1$. Thus, we construct the composite POCS operator as a cascade action of three operators. Hence, the action of such $\mathcal{P}$ is threefold. First, the local statistics-based despeckling filter [1, 12, 24] $\mathcal{P}_1 = \mathcal{P}_{desp}$ transforms the speckle corrupted MSF image $\mathbf{g} = \{\mathbf{q}\mathbf{q}^{+}\}_{\text{diag}}$ into the despeckled low resolution image $\hat{\mathbf{b}}_{despMSF} = \hat{\mathbf{b}}_{[0]} = \mathcal{P}_{desp}\{\mathbf{g}\}$ that serves as an input (the zero-step iteration $\hat{\mathbf{b}}_{[0]}$) for the further iterative reconstructive processing.

Second, $\mathcal{P}_2$ transforms (29) into the implicit contractive mapping iterative scheme, i.e., $\mathcal{P}_2 = \mathcal{P}_{iter}$, with two corresponding discrepancy terms related to the $\ell_2 - \ell_2$ structured metric specified by (12). Last, $\mathcal{P}_3 = \mathcal{P}_{\pi}$ acts as a hard threshholding operator that at each iteration $i = 1, \ldots$ clips off all entries of $\hat{\mathbf{b}}_{[i]}$ lower than the user specified nonnegative sparsity preserving tolerance threshold level π.

From the fundamental theorem of POCS [11] it follows that composite $\mathcal{P}_{\pi}\mathcal{P}_{iter}$ serves also as a convergence guaranteed POCS operator. With such cascade $\mathcal{P}$ the (32) is transformed into the implicit iterative feature enhanced DEDR-MVDR technique

$$\hat{\mathbf{b}}_{[i+1]} = \mathcal{P}_{\pi}\{\hat{\mathbf{b}}_{[i]} + \lambda_1(\mathbf{f}_{[i]} - \mathbf{\Phi}_{[i]}\hat{\mathbf{b}}_{[i]}) + \lambda_2\nabla^{2}[\mathbf{f}_{[i]} - (\mathbf{\Phi}_{[i]}\hat{\mathbf{b}}_{[i]})]\} \qquad (33)$$

different from all other competing approaches [1–14]. Instead of equibalanced $\ell_2 - \ell_2$ weights specified in (12),

here we have incorporated two regularization factors (hyperparameters) λ_1, λ_2 that balance the relative contribution of two $\ell_2 - \ell_2$ metrics structured discrepancy terms in (33). The simplest equibalanced model assumes $\lambda_1 = \lambda_2 = 1$. The iterative process is initialized with $\hat{\mathbf{b}}_{[0]} = \mathcal{P}_{desp}\mathbf{g}$ and is terminated at $\hat{\mathbf{b}}_{[I]}$ for which the user specified convergence tolerance level ε is attained at some $i = I$ or the maximal admissible number of iterations I is performed. In the simulations reported in the next Section, we have adopted ε = 0.05 with balanced $\lambda_1 = 1$, $\lambda_2 = 0.5$.

B. Schematic- Form Implementation Structure

To construct the schematic processing implementation structure of the POCS-regularized DEDR-MVDR technique (32), (33) we make the use of the operator feedback loop structure of Figure 3(a) that yields the composite transfer matrix

$$\mathbf{A} = (\mathbf{A}_1\mathbf{A}_2 + k\mathbf{I})^{-1}\mathbf{A}_1 . \quad (34)$$

With the specifications, $k = N_\Sigma$, $\mathbf{A}_1 = \mathbf{D}(\hat{\mathbf{b}}_{[i]})$ and with $\mathbf{A}_2 = \mathbf{\Psi}$, this scheme is exactly suited to perform the computing operations required by the solver (32), (33). The schematic-form computational structure of the resulting iterative POCS-regularized DEDR-MVDR technique (33) is presented in Figure 3(b).

It is worthwhile to note that the constructed implementation scheme of Figure. 3(b) does not involve matrix inversions at all processing levels. Also, incorporation of the sparsity preserving POCS operator $\mathcal{P}_3 = \mathcal{P}_\pi$ speeds-up the overall iterative process as we next corroborate in the simulations reported in Section V. These two aspects constitute significant advantages of the developed DEDR-MVDR method for feature enhanced SSP vector recovery.

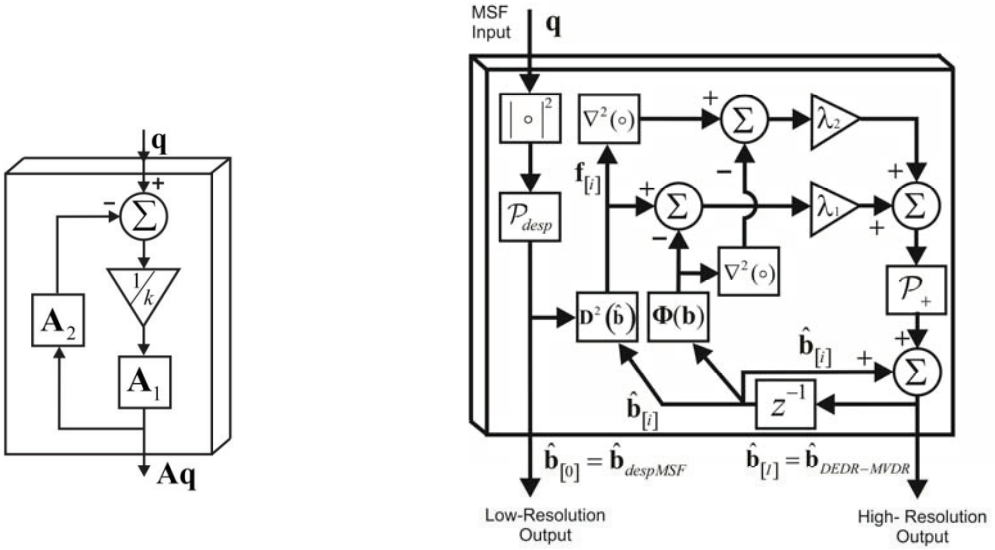

(a) (b)

Fig. 3 (a) Feedback loop structure of operator **A** defined by (34); (b) Double feedback loop-type implicit iterative algorithmic structure of the sparsity preserving DEDR-MVDR technique. Block labeled by $|\circ|^2$ defines the element-wise square detection operator, block labeled by z^{-1} defines the one step delay operator.

IV. NUMERICAL SIMULATIONS

A. Simulation Details

In the simulations, we treated a conventional F-SAR system under typical system specifications, the same as in the comparative previous studies [9, 12, 13]. Following such specifications, we considered the 1024×1024 pixel-framed scene and adopted triangular shape of the imaging F-SAR slant range ambiguity function and Gaussian shape of the corresponding azimuth MSF ambiguity function. The degradations at the image formation level due to the SFO uncertainties were simulated using the statistical model of a SAR image defocusing [3, 4, 8]. The fractional resolution along the x (azimuth) and y (range) scene coordinates were controlled by assigning different effective pixel widths k_r and k_a of the range and the azimuth PSFs and their varying over the scene that account to the range variation effect [4]. To comply with the technically motivated MSF fractional image the SFO uncertainty was simulated adopting the fully developed speckle model (single-look F-SAR modality) from the comparative studies [1, 9, 12], i.e., the blurred scene image was degraded with the composite (signal-dependent) noise simulated as a realization of χ_2^2-distributed random variables with the pixel mean value assigned to the actual degraded scene image pixel, i.e., zero dB signal-to-noise ratio, SNR = 0 dB [4]. Such degradations encompass both uncontrolled SFO distortions and MSF mismatches attributed to propagation medium perturbations and uncompensated carrier trajectory deviations that may occur in some severe operational scenarios [2, 4, 13].

The simulation experiment compares the developed DEDR-MVDR technique (33) implemented via the structural processing using the scheme of Figure 3(b) with two most prominent competing SAR-adapted enhanced imaging techniques, namely: the celebrated variational analysis (VA) inspired anisotropic diffusion (AD) method [16, 20, 23] adapted to SAR imaging in [12, 13], and the advanced modified robust adaptive spatial filtering (RASF)

method of [13] that does not involve the image gradient norm in the ℓ_2 only structured image space.

B. Quantitative Performance Metrics

In order to quantitatively evaluate the image enhancement performances obtained with different compared employed reconstruction methods, we have employed three performance metrics commonly used in the image analysis applications [1, 19, 21, 22]. The first one, is the so-called improvement in the output signal-to-noise ratio (IOSNR) measured via the ratio of the corresponding squared ℓ_2 error norms defined as [12, 19]

$$IOSNR^{(\mathrm{p})} = 10\log_{10}\left(\left\|\mathbf{g}-\mathbf{b}\right\|^2 \Big/ \left\|\hat{\mathbf{b}}^{(p)}-\mathbf{b}\right\|^2\right) \qquad (35)$$

where $\mathbf{b}$ represents the original SSP frame, $\mathbf{g}$ is the low-resolution speckle-corrupted image formed by a fractional SAR system that employs the conventional MSF method (28), and $\hat{\mathbf{b}}^{(p)}$ represents the SSP reconstructed from the corrupted MSF image $\mathbf{g}$ applying the pth imaging method from the simulated family (p = 1, 2, 3, 4): p = 1 corresponds to the original low resolution MSF image $\hat{\mathbf{b}}^{(1)} = \mathbf{g}$; p = 2 corresponds to the image enhanced with the celebrated non-parametric model-free anisotropic diffusion (AD) procedure adapted to SAR imaging [12, 13]; p = 3 relates to the image recovered employing the most prominent competing DEDR-related RASF algorithm [13]; p = 4 corresponds to the feature enhanced image reconstruction performed with the developed here DEDR-MVDR method.

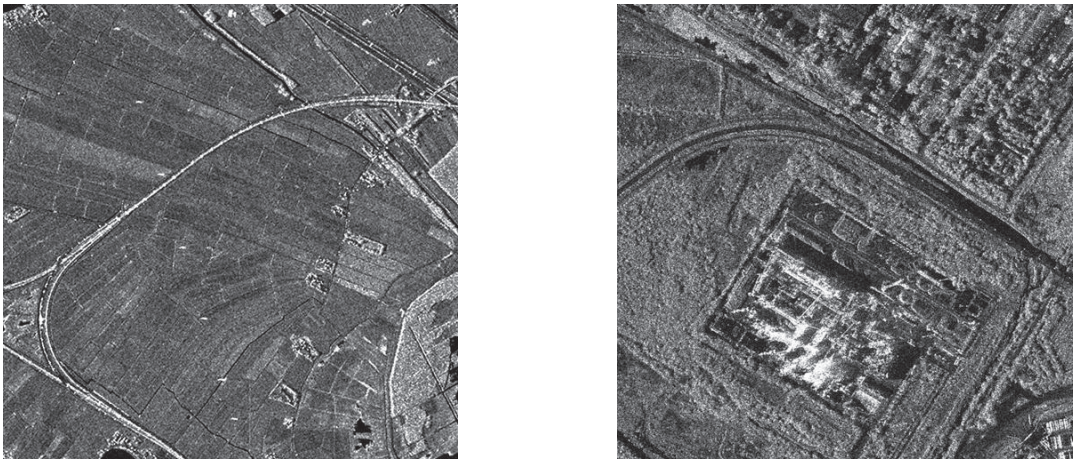

(a) (b)

Fig. 4. Original scene for the first and second scenarios (not observable with the simulated F-SAR systems).

The second quantitative evaluation metric is the mean absolute error (MAE)

$$MAE^{(\mathrm{p})} = 10\log_{10}\left\{\frac{1}{K_x K_y}\sum_{k_x=1}^{K_x}\sum_{k_y=1}^{K_y}\left|\hat{b}^{(p)}\left(k_x,k_y\right)-b\left(k_x,k_y\right)\right|\right\} \qquad (36)$$

where $\{b(k_x,k_y)\}$ represent the pixel values of the initial SSP and $\{\hat{b}^{(p)}(k_x,k_y)\}$ represent the pixel values of the SSP reconstructed applying the pth tested technique (p = 1, 2, 3, 4). As a note, this metric is well suitable for quantification of fine image reconstruction details, such as edge preservation (sharpening) and resolution of small targets on the extended scene [19, 21].

Finally, the third employed quality metric is the so-called structural similarity index measure (SSIM). The SSIM quantifies the perceptual difference between the distorted image and the reference image. It was originally designed in [21, 22] as a quantitative measure that closely emulates the human visual system. Following [21, 22], the structural information in an image relates to those attributes that represent the structure of objects in the scene independent of the average luminance and contrast. The mean squared error (MSE) and the peak signal-to-noise ratio (PSNR) quality metrics might not be well matched to perceived visual quality. Two distorted images with the same or close MSE and PSNR may have very different types of errors, some of which are much more visible than others. That is why; SSIM is a better indicator of perceived image quality. It is defined as follows [21, 22]

$$\mathrm{SSIM}\left(\mathbf{b},\hat{\mathbf{b}}^{(p)}\right) = \frac{\left(2\mu_{\mathbf{b}}\mu_{\hat{\mathbf{b}}^{(p)}}+C_1\right)\left(2\sigma_{\mathbf{b}\hat{\mathbf{b}}_{[i]}}+C_2\right)}{\left(\mu_{\mathbf{b}}{}^2+\mu_{\hat{\mathbf{b}}^{(p)}}{}^2+C_1\right)\left(\sigma_{\mathbf{b}}{}^2+\sigma_{\hat{\mathbf{b}}^{(p)}}{}^2+C_2\right)} \qquad (37)$$

where, as in (35), $\mathbf{b}$ represents the original SSP frame and $\hat{\mathbf{b}}^{(p)}$ is the SSP estimate formed applying the corresponding pth method from the tested family (p = 1, …, 4), and coefficients C_1, C_2 are included to avoid instability [21, 22]. In (37), the image luminance is estimated as the mean intensity

$$\mu_{\mathbf{x}} = \frac{1}{K}\sum_{k=1}^{K} x_k; \qquad (38)$$

the standard deviation

$$\sigma_{\mathbf{x}} = \left(\frac{1}{K}\sum_{k=1}^{K}\left(x_k-\mu_{\mathbf{x}}\right)^2\right)^{\frac{1}{2}} \qquad (39)$$

is used as an estimate of the image contrast, and the structure comparison is performed via evaluating the covariance between the corresponding compared images

$$\sigma^2_{\mathbf{x},\mathbf{y}} = \frac{1}{K}\sum_{k=1}^{K}\left(x_k-\mu_{\mathbf{x}}\right)\left(y_k-\mu_{\mathbf{y}}\right). \qquad (40)$$

In the simulations reported in the next Section, we have used C_1 = 1e-4 and C_2 = 9e-4 following the structure suggested in [21, 22].

C. Simulation Results and Discussion

Figure 4 presents the high resolution despeckled scene image formed with a hypothetical full-focused SAR (not observable with the simulated F-SAR) for two scenes borrowed from the real-world SAR imagery [26].

The low resolution speckle corrupted scene images in Figure 5(a) and in Figure 6(a) correspond to the simulated single look F-SAR (quick look modality (25), (28)) for the operational scenario specifications similar to those from the competing studies [1, 9, 13] as specified in the Figure captions. Figures 5(b) thru 5(d) and Figures 6(b) thru 6(d) report the feature-enhanced radar imaging results obtained with different compared DEDR-related techniques as specified in the Figure captions. These results verify that the best perceptual F-SAR image enhancement performances as well as convergence rates were attained with the developed POCS regularized DEDR-MVDR method. In the first scenario related to the scene shown in Figure 4(a), the simulated degradations in the resolution are moderate over the range direction (κ_r = 10) and significantly larger over the azimuth direction (κ_a = 20). In the second scenario related to the scene shown in Figure 4(b), the fractional SAR system suffers from much more severe degradations due to additional defocusing in both directions (κ_r = 15; κ_a = 30). Next, Figures 5(b) and 6(b) show the images enhanced applying the competing anisotropic diffusion (AD) technique [16, 23]. The images reconstructed using the competing DEDR-related RASF method [12] are shown in Figures 5(c) and 6(c), and the corresponding images optimally reconstructed applying the developed here DEDR-MVDR technique (after 12…14 performed iterations) are presented in Figures 5(d) and 6(d), respectively.

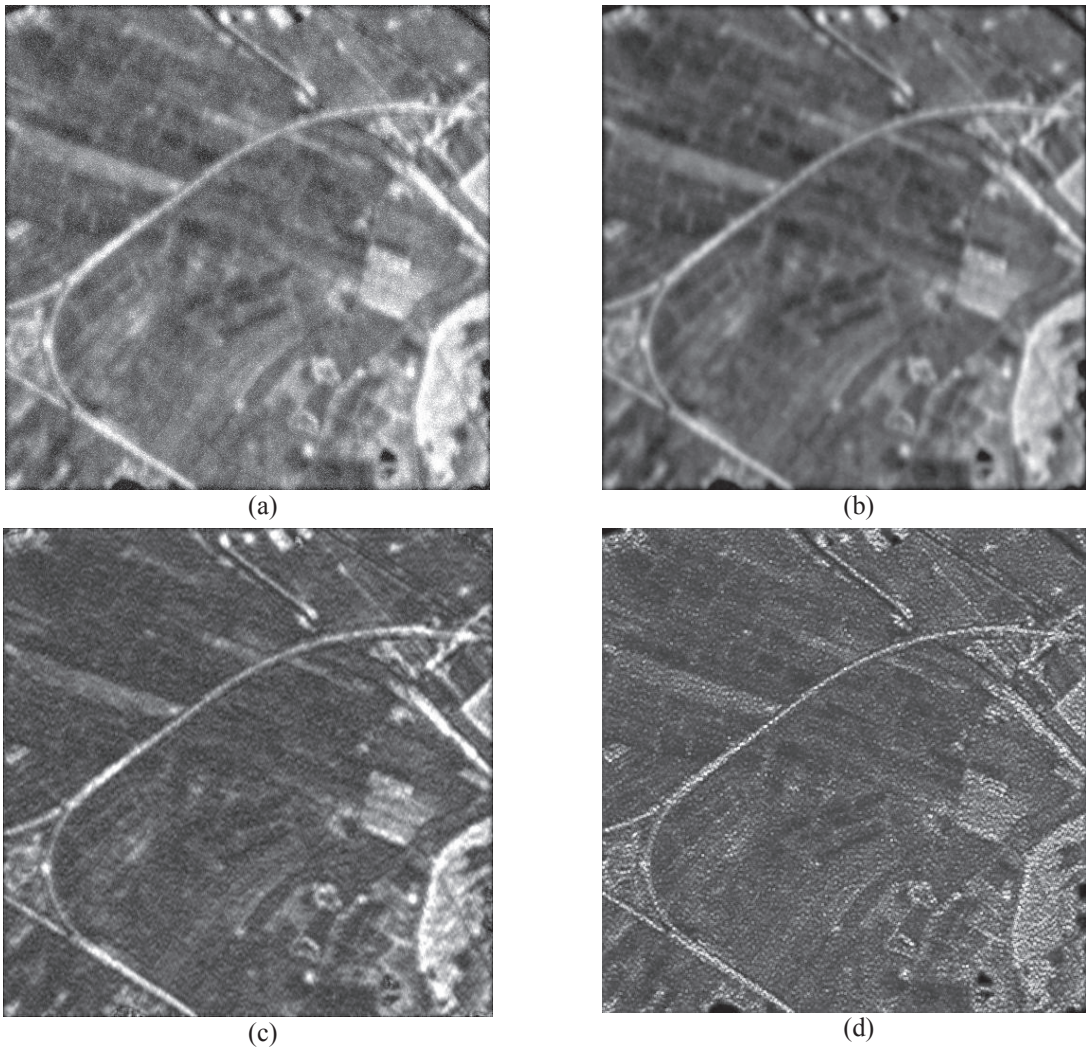

Fig. 5. Simulation results for four tested imaging modalities: (a) low resolution speckle corrupted MSF image of the first scene formed with a simulated F-SAR system; modeled system parameters: squared triangular range point spread function (PSF), the width (at ½ of the peak value) κ_y = 10 pixels; squared Gaussian bell azimuth PSF, the width (at ½ of the peak value) κ_x = 20 pixels; the worst case single-look scenario with fully developed speckle, (SNR = 0 dB); (b) the same scene image enhanced using the AD technique (convergence at 43 iterations); (c) result of reconstructive imaging performed with the DEDR-related RASF method (convergence at 34 iterations); (d) the same image reconstructed applying the developed here DEDR-MVDR technique (convergence at 12 iterations). All results are reported for the zero-level threshold π = 0.

Table 1 reports the quantitative performances evaluated via three quality metrics (27), (28) and (29) obtained with three tested DEDR-related feature enhanced SSP estimation methods. Those are also indicative of the superior quantitative recovery performances attained with the proposed DEDR-MVDR technique.

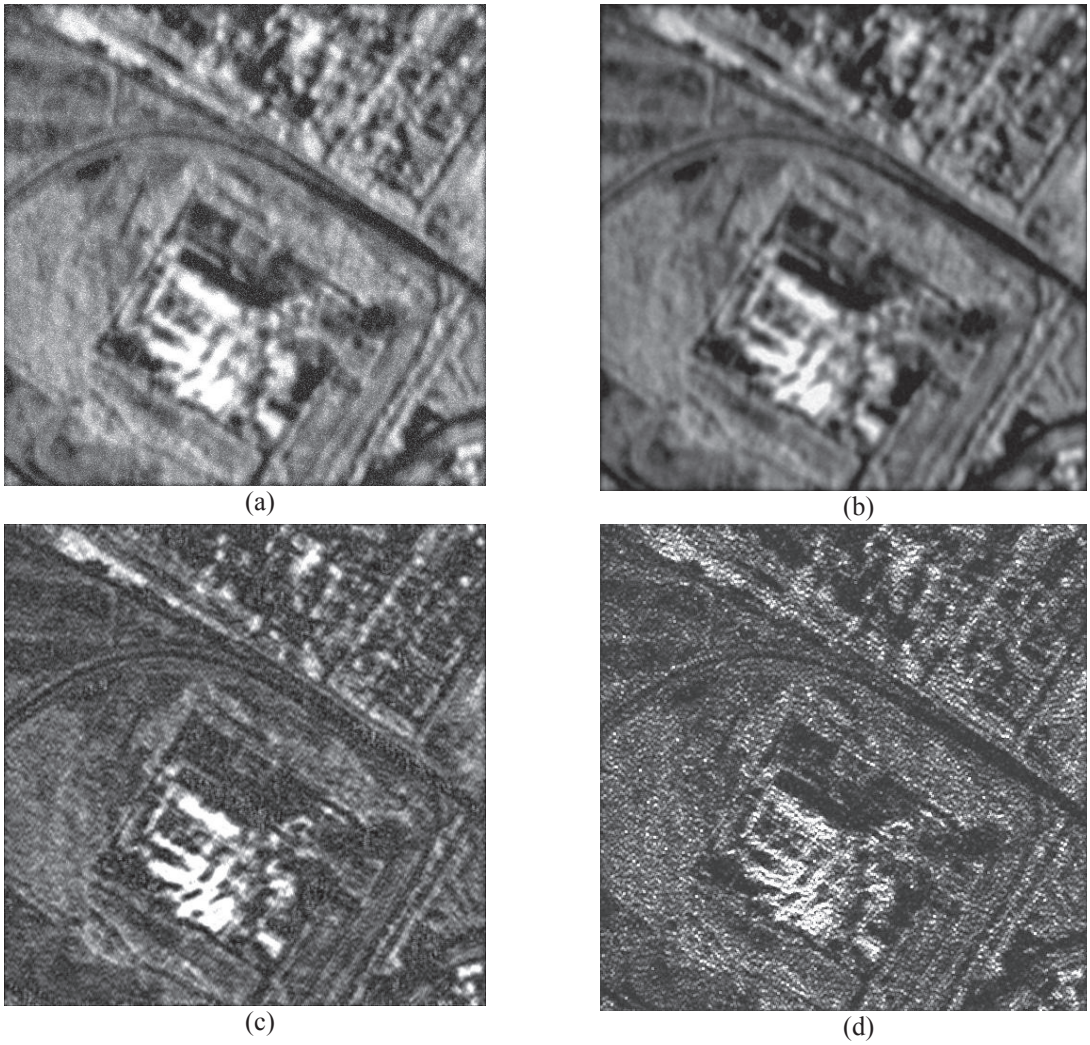

Fig. 6. Simulation results for four tested imaging modalities: (a) low resolution speckle corrupted MSF image of the second scene formed with a simulated F-SAR system; modeled system parameters: squared triangular range point spread function (PSF), the width (at ½ of the peak value) $\kappa_y = 15$ pixels; squared Gaussian bell azimuth PSF, the width (at ½ of the peak value) $\kappa_x = 30$ pixels; the worst case single-look scenario with fully developed speckle, (SNR = 0 dB); (b) the same scene image enhanced using the AD technique (convergence at 44 iterations); (c) result of reconstructive imaging performed with the DEDR-related RASF method (convergence at 36 iterations); (d) the same image reconstructed applying the fused MVDR-POCS technique (convergence at 14 performed iterations). All results are reported for the zero-level threshold $\pi = 0$.

Table 1: Quantitative results obtained for the two simulated scenarios using three different quality metrics.

	First scenario			Second scenario		
	$\kappa_y = 10$	$\kappa_x = 20$		$\kappa_y = 15$	$\kappa_x = 30$	
	IOSNR(dB)	MAE(dB)	SSIM	IOSNR(dB)	MAE(dB)	SSIM
AD	2.61	18.91	0.42	2.18	18.83	0.37
RASF	2.75	18.70	0.42	2.32	18.59	0.45
DEDR-MVDR	3.51	18.65	0.49	3.05	18.59	0.56

V. Conclusion

In this paper, we have treated the feature enhanced RS imaging problem particularly adapted to the conventional RAR/F-SAR sensors. The image recovery problem was casted and treated in the inverse problem statement as an enhanced resolution reconstruction of the desired SSP of the remotely sensed scene from the low resolution MSF image. The solution to the inverse problem at hand was derived based on the generic DEDR framework. The DEDR solution strategy does not require a priori knowledge of the data signal statistical distributions and is aimed at the optimal balancing of the adaptive resolution enhancement over the spatially selective composite noise suppression (both additive noise and multiplicative speckle). To find an efficient solution, we have performed the DEDR restructuring of the celebrated robust MVDR virtual beamforming-based high resolution SSP reconstruction technique particularly adapted to the RAR/F-SAR sensing modalities that yields the new unified DEDR-MVDR-optimal inverse problem solver. The developed DEDR-MVDR method manifests considerably

enhanced SSP reconstruction features. It outperforms the prominent competing high-resolution imaging techniques in the perceptual image recovery quality as well as in the attainable quantitative performance enhancement measures. Those are achieved due to incorporation into the DEDR solution framework the edge preserving and sparsity promoting POCS regularization levels. Moreover, due to the employed composite POCS regularization the DEDR-MVDR enhanced radar imaging technique is implementable in a considerably speeded-up implicit iterative mode that completely excludes cumbersome matrix inversions at all processing stages. The new DEDR-MVDR method does not need the observer's supervision, facilitates parallel processing and manifests super-resolution performances that make it a viable candidate for perspective digital-form implementation in low cost RAR/F-SAR sensing instruments.

REFERENCES

[1] *Shkvarko, Y.V., Amao J.A.,* Descriptive Experiment Design Restructured MVDR Beamforming Technique for Enhanced Imaging with Unfocused SAR Systems, Progress in Pattern Recognition, Image Analysis, Computer Vision, and Applications Lecture Notes in Computer Science Volume 8827, Springer, pp. 965-972, 2014.

[2] *Curlander, J. C., McDonough, R.,* Synthetic Aperture Radar – System and Signal Processing, NY, Wiley, 1991.

[3] *Henderson, F.M., Lewis, A. V. Eds.:* Principles and Applications of Imaging Radar, Manual of Remote Sensing, 3rd Ed (3), NY: Willey, 1998.

[4] *Cumming, I.G., Wong, F.H.,* Digital Processing of Synthetic Aperture Radar, Artech House. 1st edition, 2005.

[5] *Ishimary, A.,* Wave Propagation and Scattering in Random Media, NY, IEEE Press, 1997.

[6] *Farina, A.,* Antenna-Based Signal Processing Techniques for Radar Systems, Norwood, MA, Artech House, 1991.

[7] *Patel, V.M., Easley, G.R., Healy, D.M., Chellappa, R.,* Compressed synthetic aperture radar, IEEE Journal of Selected Topics in Signal Proc 4(2), 244-254, 2010.

[8] *L.G. Cutrona,* Synthetic aperture radar, in Radar Handbook, 2nd ed, M.I. Skolnic,Ed. n chief, MA, McGraw Hills, pp.21.1–21.23, 1990.

[9] *Shkvarko, Y.V., Tuxpan, J., Santos, S.R.,* High-resolution imaging with uncertain radar measurement data: A doubly regularized compressive sensing experiment design approach, in Proc. IEEE 2012 IGARSS Symposium, ISBN: 978-1-467311-51/12, 6976-6970, 2012.

[10] *Yarbidi, T., Li, J., Stoica, P., Xue, M., Baggeroer, A.B.,* Source localization and sensing: A nonparametric iterative adaptive approach based on weighted least squares, IEEE Trans. Aerospace and Electronic Syst. 46(1), 425.443, 2010.

[11] *Barrett, H.H., Myers, K.J.,* Foundations of Image Science, NY, Willey, 2004.

[12] *Shkvarko, Y.V.,* Unifying experiment design and convex regularization techniques for enhanced imaging with uncertain remote sensing data. — Part I: Theory; — Part II: Adaptive implementation and performance issues, IEEE Trans. Geoscience and Remote Sensing 48(1), 82-111, 2010.

[13] *Shkvarko, Y.V, Tuxpan, J., Santos, S.R.*, Dynamic experiment design regularization approach to adaptive imaging with array radar/SAR sensor systems, Sensors 11, 4483-4511, 2011.

[14] *Krieger, G.,* MIMO-SAR:Opportunities and Pitfalls, IEEE Transactions on Geoscience and Remote Sensing Vol. 52, No. 5, pp. 2628-2645, 2014.

[15] *Zibulevsky, M.,* Elad, M., L1-L2 Optimization in Signal and Image Processing, IEEE Signal Processing Magazine, Vol. 27, Issue 3, pp. 76-88, May 2010.

[16] *Black, M.J., Shapiro, G., Marimont, D.H., Heeger, D.,* Robust anisotropic diffusion, IEEE Trans. Image Proc., vol. 7, No. 3, pp. 421-432, 1998.

[17] *Campisi, P., Egiazarian, K.,* Blind Image Deconvolution: Theory and Applications, NY, CRC Press, 2007.

[18] *Li, J., Stoica, P.,* Robust Adaptive Beamforming, NY, Wiley, 2006.

[19] *Perry, S.W., Wong. H.S., Guan, L.,* Adaptive Image Processing, NY, CRS Press, 2001.

[20] *John, S., Vorontsov, M.A.,* Multiframe selective information fusion from robust error theory, IEEE Trans. Image Proc., Vol. 14, No. 5, pp. 577-584, 2005.

[21] *Horé, A., Ziou, D.,* Image quality metrics: PSNR vs. SSIM, 20th International Conference on Pattern Recognition, pp. 2366-2369, 2010.

[22] *Zhou Wang, Alan C. Bovik, Hamid R.* Sheikh and Eero P. Simoncelli. Image Quality Assessment: From Error Visibility to Structural Similarity, IEEE Trans. Image Proc., Vol. 13, pp.600-612, 2004.

[23] *Perona, P.; Malik, J.* Scale-space and edge detection using anisotropic diffusion, IEEE Trans. Pattern Anal. Machine Intell. 12, pp. 629-639, 1990.

[24] *Massonnet, D., Souyris, J.C.,* Imaging with Synthetic Aperture Radar, EPFL Press. 1st Edition, 2008.

[25] *Matthews, J.H.,* Numerical Methods for Mathematics, Science, and Engineering, Second Edition, Englewood Cliffs, NJ, Prentice Hall, 1992.

[26] "TerraSAR-X" imagery, Available at: http://www.astrium-geo.com/es/570-galeria-de-imagenes?img

Manuscript received March, 18, 2016

Yuriy V. Shkvarko (M'95–SM'04) received the Dip. Eng. (Hon.) degree in electrical engineering in 1976, the Ph.D. degree in radio engineering in 1980, and the Doctor of Science degree in radio physics, radar and navigation in 1990, all from the Kharkov Aviation Institute, Ukraine, the ex USSR. From 1976 to 1991, he was with the Scientific Research Department of the Kharkov Aviation Institute, Kharkov, ex USSR, as a Research Fellow, Senior Fellow and finally as a Chair of the Research Laboratory in information technologies for radar and navigation. From 1991 to 1999 he was a Full Professor at the Department of System Analysis and Control of the Ukrainian National Polytechnic Institute at Kharkov, Ukraine. He immigrated to Mexico in 1999. From 1999 to 2001 he was an invited professor at the Guanajuato State University at Salamanca, Mexico. In 2001, he joined CINVESTAV del IPN (superior education and research center of the National Polytechnic Institute of Mexico) at Guadalajara, Mexico as a Full Titular Professor. Dr. Shkvarko holds 12 patents and has published two books and some 190 journal and conference papers. His research interests are in applications of signal processing to remote sensing, imaging radar, navigation and communications, particularly in inverse problems, random fields estimation, adaptive spatial analysis, statistical sensor array and multimode remote sensing data processing, and knowledge-aided system fusion.

Joel A. Amao received the Dip. Eng. degree in Electronics and Communications from the University of Guadalajara, Mexico, in 2012 and the M.S. degree in Electrical Engineering from the CINVESTAV del IPN (superior education and research center of the National Polytechnic Institute of Mexico) at Guadalajara, Mexico, in 2014. Currently, he is working towards the Ph.D. degree in Electrical Engineering at the telecom-munications division of the CINVESTAV del IPN at Guadalajara, Mexico. His research interests include digital signal and image processing for remote sensing applications and high resolution computational imaging.

Juan I. Yanez (M'12) received the Dip. Eng. degree in Electronics and Communications in 2008 and the Master in Engineering degree in 2011, both from the University of Guanajuato, Guanajuato, Mexico. From 2010 to 2011 he was an assistance professor at the Electronics Department, Division of Engineering, at the University of Guanajuato, Mexico. Currently, he is working towards the Ph.D. degree in Electrical Engineering at the telecommunications division of the CINVESTAV del IPN at Guadalajara, Mexico. His research interests include applied digital signal and image processing for remote sensing and neural network computing based sensor data fusion for imaging radar.

УДК 621.396

Формирование высокоразрешающих радиолокационных и РСА изображений: регуляризационный подход на основе виртуального диаграммообразования / Ю.В. Шкварко, Х.А. Амао, Х.И. Яньез // Прикладная радиоэлектроника: научн.-техн. журнал. – 2016. – Том 15. – № 1. – С. 26–38.

Для информационного анализа данных дистанционного зондирования, формируемых обычными радиолокационными системами бокового обзора (РЛС-БО) и радиолокаторами с неполной (фракционно) синтезированной апертурой (Ф-РСА), первичные радиолокационные изображения (РЛИ) с низким разрешением, зашумленные спеклом, должны быть дополнительно обработаны для повышения их качества. В предлагаемой работе эта проблема решается в контексте обратных задач высокоразрешающей реставрации радиояркостных изображений зондируемых сцен из первичных спеклзашумленных РЛИ низкого разрешения. Вначале, следуя методологии регуляризации на основе дескриптивного планирования эксперимента (РДПЭ), метод виртуального адаптивного диаграммообразования Кейпона (минимальной вариации без смещения (МВБС)) адаптируется к задаче реконструкции РЛИ. Далее, в РДПЭ-реструктуированный МВБС вводятся дополнительные регуляризационные уровни проекций на выпуклые множества (ПВМ), ориентированные на обеспечение сходимости реставрационной итерационной схемы и поддержку возможной разреженности (*sparsity*) в результирующем реконструированном РЛИ. Введение многоуровневых ПВМ в РДПЭ-оптимально реструктурированную МВБС схему приводит к новому методу реставрации РЛИ (адресованному как РДПЭ-МВБС), который обеспечивает существенное улучшение качества реконструкции изображения за счет пространственно селективного адаптивного подавления спекла РДПЭ-оптимально сбалансированного с повышением разрешения и поддержкой *sparsity*. Вычислительно, предложенный РДПЭ-МВБС метод реализован в виде неявной итерационной схемы полностью исключающей обращения матриц на всех этапах реконструктивной обработки РЛИ. Приведенные данные численного моделирования подтверждают более высокую эффективность предложенного РДПЭ-МВБС метода в сравнении с другими конкурирующими непараметрическими адаптивными методами повышения качества РЛИ.

Ключевые слова: диаграммообразование, регуляризация на основе дескриптивного планирования эксперимента (РДПЭ), радиолокатор с синтезированной апертурой (РСА), радиолокационное изображение, разрешение.

Табл. 1. Рис. 6 . Библиогр.: 26 назв.

УДК 621.396

Формування надрозділяючих радіолокаційних та РСА зображень: регуляризаційний підхід на базі віртуального діаграмостворення / Ю.В. Шкварко, Х.А. Амао, Х.И. Яньез // Прикладна радіоелектроніка: наук.-техн. журнал. – 2016. – Том 15. – № 1. – С. 26–38.

Для інформаційного аналізу даних дистанційного зондування, що формуються звичайними радіолокаційними системами бокового огляду (РЛС-БО) та радіолокаторами з частково (фракційно) синтезованою апертурою (Ф-РСА), первинні радіолокаційні зображення (РЛЗ) з низьким розділенням, зашумлені спеклом, повинні додатково оброблятися для підвищення їх якості. В роботі, що пропонується, ця проблема вирішується в контексті обернених задач надрозділяючої реставрації радіояскравих зображень сцен, що зондуються, з первинних спеклзашумлених РЛЗ низького розділення. Спочатку, виходячи з методології регуляризації на базі дескриптивного планування експерименту (РДПЕ), метод віртуального адаптивного діаграмостворення Кейпона (мінімальної варіації без зсуву (МВБЗ)) адаптується до задачі реконструкції РЛЗ. Далі, в РДПЕ – реструктурованій МВБЗ вводяться додаткові регуляризаційні рівні проєкцій на випуклі множини (ПВМ), зорієнтовані на забезпечення збігу реставраційної ітераційної схеми та підтримку можливого розрідження (*sparsity*) в результуючому реконструйованому РЛЗ. Введення багаторівневих ПВМ в РДПЕ – оптимальну реструктуровану МВБЗ схему дає новий метод реставрації РЛЗ (визначений як РДПЕ-МВБЗ), який забезпечує істотне підвищення якості реконструкції зображень за рахунок просторово селективного адаптивного заглушення спекла РДПЕ – оптимально збалансованого з підвищеним розділенням та підтримкою розрідження. Обчислювально запропонований РДПЕ – МВБЗ метод реалізовано у вигляді неявної ітераційної схеми, яка повністю виключає обернення матриць на всіх етапах реконструктивної обробки РЛЗ. Наведені результати математичного моделювання підтверджують більш високу ефективність запропонованого РДПЕ- МВБЗ методу порівняно з іншими конкуруючими непараметричними адаптивними методами підвищення якості РЛЗ.

Ключові слова: діаграмостворення, регуляризації на базі дескриптивного планування експерименту (РДПЕ), радіолокатор з синтезованою апертурою (РСА), радіолокаційне зображення, розділення.

Табл. 1. Рис. 6. Бібліогр.: 26 найм.